Comparison of Thyristor-Controlled Rectification Topologies for a Six-Phase Rotating Brushless Permanent Magnet Exciter

Nøland, J.K.[1], Hjelmervik, K.B.[1], Lundin, U.[2]
[1]University College of Southeast-Norway, Norway
[2]Uppsala University, Sweden

IEEE Transactions on Energy Conversion 2016, 31(1), 314-322

doi: 10.1109/TEC.2015.2480884

Comparison of Thyristor-Controlled Rectification Topologies for a Six-Phase Rotating Brushless Permanent Magnet Exciter

Jonas Kristiansen Nøland, *Student Member, IEEE,* Karina Bakkeløkken Hjelmervik and Urban Lundin

***Abstract*—The thyristor bridge rectifier has proven to be a reliable solution regarding control of excitation equipment for synchronous generators. However, in rotating brushless exciters the diode rectifier is the dominant topology on the shaft. In order to improve the step response of rotating exciters, one could put a thyristor bridge rectifier on the rotating part and control the firing angle remotely from a stationary controller. This paper compares different multiphase configurations of permanent magnet synchronous machines as a rotating exciter and the possibility to reduce the torque ripple by selecting the appropriate rectification topology. The paper also explains the implications of the self and mutual inductances of the armature windings for the performance of the exciter.**

***Index Terms*—Brushless exciters, rotating exciters, permanent magnet machines, synchronous generators, active rectification, controlled excitation, voltage stability.**

I. Introduction

VOLTAGE stability on an interconnected AC-grid is directly dependent on the dynamic performance of the excitation equipment for synchronously connected generators and motors. The excitation system of synchronous generators is either static or rotating [1]. The static system feeds direct current (DC) to the rotor through brushes. The conventional rotating system consists of an excitation machine fed by controllable field windings on the exciter stator and a rotating armature winding on the rotor [2]. Instead of having a diode rectifier on the rotating shaft, it is possible to combine the advantages of a rotating brushless exciter, such as low maintenance need, with the fast response of a static exciter by replacing the diodes mounted on the shaft with an active rectification system. The simplest implementation consists of a 6-pulse thyristor rectification bridge [3]. In such a system, one has to transfer a control signal to the shaft and thereby maneuver the thyristors.

By direct thyristor rectification of the exciter armature voltages on the shaft, the step response of the excitation current can be enhanced compared to conventional systems. This is necessary in order to enable the grid-connected brushless synchronous generator to fulfill the step response requirements of the grid, and improve the low voltage faults ride through. By means of remote adjustments of the thyristor firing angles on the shaft, the generator field winding can directly sense a change in the average output DC voltage from the exciter. The thyristor bridge rectifier is already a reliable solution regarding control of excitation equipment for synchronous generators [4], however it is rarely found on the rotating shaft.

A pilot test of such an active rotating excitation system, with wireless Bluetooth communication between the stator and the rotor, was installed at a hydropower unit in Sweden (45MVA, 115rpm). The system worked well in operation, but vibrations were observed in the generator top cover at a higher operating firing angle on the rotating thyristor bridge. Unfortunately, the vibrations coincided with a mechanical resonance frequency on the generator top cover. However, the improved step response time of the excitation was verified.

The torque ripple is not problematic in conventional rotating exciters. In that case, one of the contributors to the excitation power is the stationary thyristor bridge connected to the stator field winding of the exciter. The stationary thyristor bridge draws its main power from the generator terminals.

It is interesting to see if one can minimize the torque pulsations already in the exciter design. Furthermore, different rectification topologies opens up possible new exciter designs. The application of permanent magnets on rotating exciters is not something new. Permanent Magnet Generators (PMGs) have been used in the past as pre-exciters, even in aircraft systems [5]. However, a three-stage system is not able to meet the fast step response requirements for larger synchronous generators. The literature includes investigations on the use of permanent magnets in two stage systems [6]. However, in hybrid two-stage systems, with permanent magnets in the stator of the exciter, the excitation control comes from an external field current fed into the stator of the exciter [7], leading to a slow step response. If all the excitation control is applied on the shaft, in the simplest form, with a rotating thyristor bridge, one would only need permanent magnets on the exciter stator, no field windings. Different thyristor rectification topologies are interesting to investigate. Earlier investigations on the use of multilevel topologies in thyristor rectification schemes shows a reduction in the harmonic content in the phase current [8], which may be beneficial for torque ripple reduction.

In order to study the impact of the rectification topologies on the performance and the torque pulsations of the exciter, both analytical and numerical models are developed. This

Work supported by Statkraft AS, Lilleakerveien, 0216 Oslo, Norway.

J. K. Nøland is with both the Department of Engineering Sciences, Division of Electricity, Uppsala University, Uppsala, 751 21 Sweden (e-mail: Jonas.Noland@angstrom.uu.se) and the Faculty of Technology and Maritime Science, Buskerud and Vestfold University College, 3184 Borre, Norway (e-mail: Jonas.Noland@hbv.no).

U. Lundin is with Uppsala University and K. B. Hjelmervik is with Buskerud and Vestfold University College.

Manuscript received April 15, 2015; revised August 7, 2015; accepted September 12, 2015.

paper presents a numerical simulation model for the exciter topologies. The model parameters are found using finite element techniques. Earlier, the same approach has been applied for diode exciters [9], [10], where higher order terms of self and mutual inductances are accounted for. This paper shows the possibility to include some higher order terms, but the inductance slot ripple and the saturation effects are neglected. Since most exciters consists of an electrically excited field winding without permanent magnets, the armature reaction is harder to model. The recent focus for exciter modeling has been the averaged lower order models [11], [12], [13]. However, with those large time scale models, one would not be able to capture the torque ripple periodicity in detail. Another difference in this paper is the use of an asymmetrical 6-phase system in opposition to the 3-phase system. The 6-phase exciter is modeled using the split phase double dq model [14].

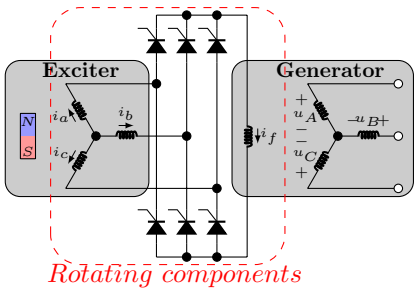

Fig. 1. Rotating thyristor bridge in a 3-phase PM excitation system

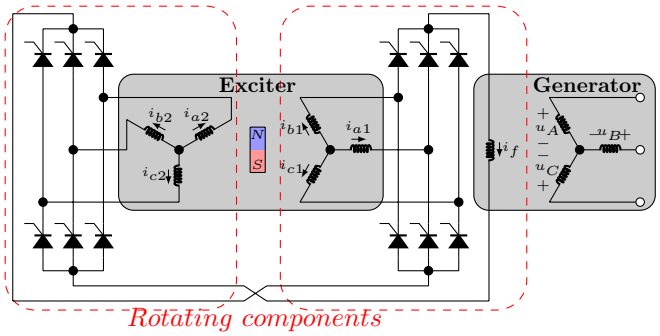

Fig. 2. Rotating multilevel thyristor bridges in a double 3-phase PM excitation system

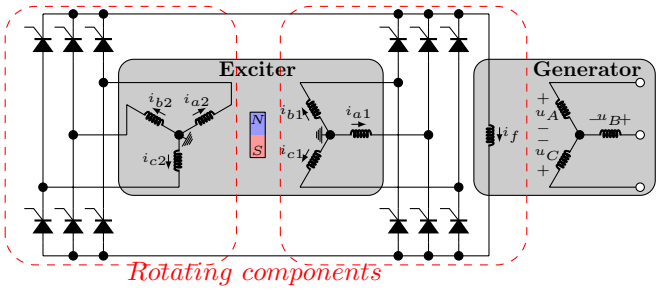

Fig. 3. Rotating parallell thyristor bridges in a 6-phase PM excitation system

The exciter could be designed either as a permanent magnet synchronous machine (PMSM) or a brushless direct current machine (BLDC). The PMSM produces sinusoidal voltages and the BLDC produces trapezoidal voltages. The PMSM and BLDC also differ in winding layout, causing the self and mutual inductance components to be different. Fig. 1, Fig. 2 and Fig. 3, shows the different thyristor rectification topologies possible for a 6-phase brushless exciter; 3-phase, double 3-phase, and 6-phase. All topologies can be connected to an exciter with an architecture equivalent to a PMSM and a BLDC, except that the BLDC is not suitable to run with the 6-phase topology because of overlapping phase voltages. The 3-phase exciter in Fig. 1 is obtained by rearranging the original 6-phase exciter windings in three series connected pairs.

An already constructed rotor of a 6-phase rotating exciter is investigated with a certain PMSM design configuration of the stator [15]. The full exciter is used to obtain parameters for a numerical model, used validate the results and conclusions obtained from an analytical model and to evaluate the proposed stator design. The final exciter will be fitted onto an in-house experimental setup [16]. Little effort is historically done on rotating exciter design, due to their small size and lower market value compared with synchronous generators [17].

II. Method

A. Analytical model

Ideally, the phase current waveform of the exciter are square wave shaped if the commutation process is neglected. The DC load is highly inductive which tends to keep the load current stiff and ripple free. The output rectifier acts as a rotating switch, switching the load current between the phases, causing the AC load to become nonlinear [18]. The thyristor bridge tends to shift the current waveform in time with a firing angle, by controlling the time when the thyristors are allowed to conduct. According to commonly accepted thyristor notation, the firing angle is defined in electrical degrees from the point in time where two phase voltages intersects in value to the point in time where they begin to exchange current. A firing pulse triggers the exchange. The perfect square wave shape is more accurate for higher firing angles of α since the driving commutation voltage is larger and therefore the commutation interval becomes small.

From the torque produced by ideal currents, the torque pulsation can be studied analytically. A measure of torque ripple can be given by the torque ripple factor [19]

$$\mathrm{TRF} = \frac{\Delta T}{T_0} = \frac{T_{max} - T_{min}}{T_0}. \quad (1)$$

In many cases, it could be convenient to use the harmonic torque to calculate the torque ripple factor [19], yielding

$$\mathrm{THD} = \frac{T_H}{T_0} = \frac{\sqrt{T_6^2 + T_{12}^2 + T_{18}^2 + \ldots}}{T_0} = \sqrt{\frac{T_{rms}^2}{T_0^2} - 1}, \quad (2)$$

which is equivalent to calculate the total harmonic distortion (THD) from sinusoidal waveforms of current and voltage [20]. Some industrial companies quantify the torque pulsation as the ratio of the harmonic torque (T_H) with respect to the nominal torque (T_N) of the designed exciter.

1) 3-phase PMSM (Fig. 1): For 3-phase diode rectification in the interval of the electrical angle (θ) from $-\frac{\pi}{6}$ to $\frac{\pi}{6}$, $i_a = 0$, $i_b = -I_{dc}$ and $i_c = I_{dc}$, where I_{dc} is the DC side load current. The amplitude-invariant dq-transformation yields

$$i_d(\theta) = \frac{2}{\sqrt{3}} I_{dc} \sin(\theta), \tag{3}$$

$$i_q(\theta) = \frac{2}{\sqrt{3}} I_{dc} \cos(\theta), \tag{4}$$

where the d-axis is aligned with the magnet pole and the q-axis is 90 electrical degrees lagging the d-axis. It is easier to relate the d- and q-currents to the electrical angle, not to the time, since the exciter rotates with the synchronous speed. It is also easier to relate the firing angle, α, to the electrical angle, θ. The firing angle causes the current waveform to be shifted, yielding a new interval from $-\frac{\pi}{6} + \alpha$ to $\frac{\pi}{6} + \alpha$, for the phase currents in phase b and c. Integrating over the new interval, the average d- and q-axis current becomes

$$i_{d,0} = \frac{2\sqrt{3}}{\pi} I_{dc} \sin(\alpha), \tag{5}$$

$$i_{q,0} = \frac{2\sqrt{3}}{\pi} I_{dc} \cos(\alpha). \tag{6}$$

Note that the average d-axis current is 0 when α is 0, which makes sense since the current waveform has no phase shift ideally at zero firing angle. The rms d- and q-axis currents becomes

$$i_{d,rms} = I_{dc} \sqrt{\frac{2}{3} - \frac{\sqrt{3}}{\pi} \cos(2\alpha)}, \tag{7}$$

$$i_{q,rms} = I_{dc} \sqrt{\frac{2}{3} + \frac{\sqrt{3}}{\pi} \cos(2\alpha)}. \tag{8}$$

If one neglects the reluctance torque contribution, the torque ripple for PMSM machines can be calculated from the analytical solutions of the q-axis current, yielding

$$THD = \sqrt{\frac{i_{q,rms}^2}{i_{q,0}^2} - 1} \tag{9}$$

2) Double 3-phase PMSM (Fig. 2): With a double 3-phase system, assuming different firing angles (α_1 and α_2), the q-axis currents in each dq system becomes

$$i_{q1}(\theta, \alpha_1) = \frac{2}{\sqrt{3}} I_{dc} \cos\left(\left[(\theta - \alpha_1) \mod \left(\frac{\pi}{3}\right)\right] - \frac{\pi}{6} + \alpha_1\right), \tag{10}$$

$$i_{q2}(\theta, \alpha_2) = \frac{2}{\sqrt{3}} I_{dc} \cos\left(\left[(\theta + \frac{\pi}{6} - \alpha_2) \mod \left(\frac{\pi}{3}\right)\right] - \frac{\pi}{6} + \alpha_2\right), \tag{11}$$

where the modulo operation, $A \mod N$, is used to return the remainder of the division of A by N. The total torque yields

$$T(\theta) = \frac{3p}{4} \psi_m \left[i_{q1}(\theta, \alpha_1) + i_{q2}(\theta, \alpha_2)\right]. \tag{12}$$

Assuming equal firing angle (α), the torque in the interval from 0 to $\frac{\pi}{6}$ becomes

$$T(\theta) = \frac{\sqrt{3}p}{2} \psi_m I_{dc} \left[cos(\theta + \alpha) + \cos\left(\theta + \alpha - \frac{\pi}{6}\right)\right]. \tag{13}$$

3) 6-phase PMSM (Fig. 3): It turns out from the no-load induced 6-phase voltages, that the natural diode commutation will happen simultaneously for the upper and bottom bridge in the 6-phase rectification system. The natural commutation frequency is $6f_0$, just as for the 3-phase system. Three line-to-line voltage pairs set up the conduction intervals, making the performance of the 6-system similar to the 3-phase system. Although the commutation frequency is the same, the commutation process is different. When the effect of the commutation is neglected, the 6-phase system shows no difference in torque ripple performance compared to the 3-phase system. The torque ripple can be derived from one of the intervals in the 6-phase rectification scheme. In the interval from $\frac{\pi}{4} + \alpha$ to $\frac{7\pi}{12} + \alpha$, phase a1, with $e_{a1} = E\sin(\theta)$, conducts the positive current, and phase b2, with $e_{b2} = E\sin(\theta - \frac{2\pi}{3} - \frac{\pi}{6})$, conducts to negative current. E is the induced phase voltage used to describe the amplitude of the no-load voltages e_{a1} and e_{b2}. The torque in the given interval becomes

$$T(\theta) = \frac{\sqrt{2+\sqrt{3}}}{2} \frac{pEI_{dc}}{\omega} \sin\left(\theta + \frac{\pi}{12}\right). \tag{14}$$

4) 3-phase BLDC: For BLDC machines, the d-axis magnet flux linkage is not ideally constant and the torque ripple cannot be calculated from the q-axis current alone. In the interval between $-\frac{\pi}{6}$ to $\frac{\pi}{6}$, the phase voltages, $e_a = \frac{6}{\pi}E\theta$, $e_b = -E$ and $e_c = E$, for the trapezoidal waveform. A dq transformation during the interval yields

$$e_d(\theta) = \frac{2}{\sqrt{3}} E \left[-\frac{2\sqrt{3}}{\pi}\theta\cos(\theta) + \sin(\theta)\right], \tag{15}$$

$$e_q(\theta) = \frac{2}{\sqrt{3}} E \left[\frac{2\sqrt{3}}{\pi}\theta\sin(\theta) + \cos(\theta)\right]. \tag{16}$$

where

$$i_d(\theta, \alpha) = \frac{2}{\sqrt{3}} I_{dc} \sin\left(\left[(\theta + \frac{\pi}{6} - \alpha) \mod \left(\frac{\pi}{3}\right)\right] - \frac{\pi}{6} + \alpha\right), \tag{17}$$

$$i_q(\theta, \alpha) = \frac{2}{\sqrt{3}} I_{dc} \cos\left(\left[(\theta + \frac{\pi}{6} - \alpha) \mod \left(\frac{\pi}{3}\right)\right] - \frac{\pi}{6} + \alpha\right). \tag{18}$$

The instantaneous torque production is then

$$T(\theta, \alpha) = \frac{3}{4}\frac{p}{\omega} \left[e_d(\theta) i_d(\theta, \alpha) + e_q(\theta) i_q(\theta, \alpha)\right]. \tag{19}$$

5) Double 3-phase BLDC: For the double 3-phase BLDC, a similar approach is used, with the double dq system, yielding

$$T(\theta, \alpha) = \frac{3}{4}\frac{p}{\omega} \left[e_{d1}(\theta) i_{d1}(\theta, \alpha) + e_{q1}(\theta) i_{q1}(\theta, \alpha) + e_{d2}(\theta) i_{d2}(\theta, \alpha) + e_{q2}(\theta) i_{q2}(\theta, \alpha)\right]. \tag{20}$$

B. Numerical model

The idealized analytical model of the exciter performance can be compared with a numerical model of a conventional winding design of a rotating exciter shown in Fig. 4. The exciter of this study is an outer pole PMSM, with stationary permanent magnets and a rotating winding armature. Design data for the exciter is shown in Table II. The load circuit is the field winding of a standard synchronous generator

with specifications given in Table I. The field winding of a synchronous generator does not act as a simple RL circuit when the generator terminals are loaded, due to the fact that the magnetic flux produced by the stator currents interacts with the field winding. However, for the unloaded case, no other currents than the excitation current flows in the generator under steady state conditions. Therefore, a simple RL circuit is valid under those assumptions.

As an input to the numerical model, model parameters are found from the 2D finite element method in COMSOL Multi-Physics, given in Table III and Table IV. The numerical model of the excitation system topologies was implemented and simulated in the SimPowerSystems package in Matlab/Simulink. The thyristor circuit elements was modeled as ideal without snubber circuits. Direct voltage measurements was used to control the firing angle from the overlapping point of the phase voltages. A self-developed double dq model controls the voltages of controlled voltage sources in the circuit and the dq model updates itself from the phase current measurements in the circuit.

The winding is distributed, causing the phases to overlap each other in space. The air gap between the rotor and stator is not comparable with conventional permanent magnet machines, causing the leakage flux to be dominant. The exciter has a large air gap in order to facilitate planned measurements. The rectangular permanent magnets are placed parallel with each other in each pole, obtaining diametrical magnetization, normally done for a PMSM design. The cogging torque is canceled out by shifting the poles one fourth of a slot pitch towards each other. As the saliency ratio of the exciter is small, the reluctance torque and the reluctance torque ripple is also neglected in the numerical model. Since the thyristor bridge is considered as the main source of the electromagnetic torque, the paper concentrates on the minimization of the torque ripple caused by the thyristors alone.

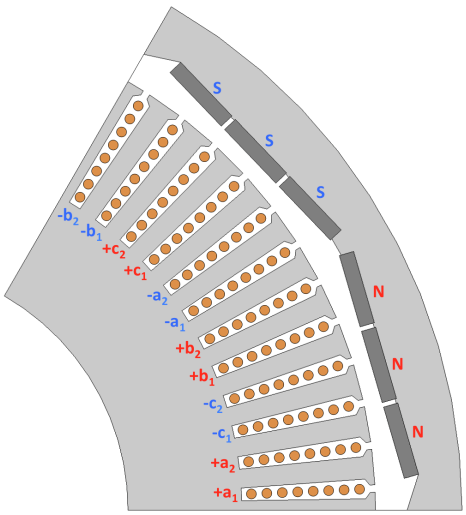

Fig. 4. 2D cross-sectional geometry of the 6-phase rotating brushless exciter

1) 3-phase connection: In order to obtain comparable peak voltages, the number of parallel-connected circuits per phase in the 3-phase connection is two. The equation system for the 3-phase exciter yields

$$u_d = \omega L_q i_q - L_d \frac{di_d}{dt} - R_s i_d \tag{21}$$

$$u_q = \omega \psi_m - \omega L_d i_d - L_q \frac{di_q}{dt} - R_s i_q, \tag{22}$$

which is the dq model, where the torque is calculated as

$$T_e = \frac{3p}{4} \psi_m i_q. \tag{23}$$

The parameters for the 3-phase model is found in Table III.

2) 6-phase connection: The 6-phase connection has originally no parallel-connected circuits (all conductors in one phase are connected in series). However for the multilevel double 3-phase connection, there exists two parallel-connected circuits per phase, which results in one fourth of the original

TABLE I
SIMULATION PARAMETERS OF THE FIELD WINDING OF THE SYNCHRONOUS GENERATOR

Symbol	Description	Value
R_f	Total load resistance	3.0Ω
L_f	Total load inductance	0.5H

TABLE II
EXCITER DESIGN SPECIFICATIONS

Parameter	Description	Value
D_o	Outer diameter	470mm
D_{si}	Inner stator diameter	425.6mm
D_{ro}	Outer rotor diameter	400mm
D_i	Inner diameter	200mm
l_a	Active length	200mm
n	Nominal speed	500rpm
ω	Electrical frequency	$100\pi \frac{rad}{s}$
m	Number of phases	6
p	Number of poles	12
Q_s	Number of slots	72
τ_s	Slot width	17.45mm
q_s	Number of slots per pole per phase	1
n_s	Number of conductors per slot	8
c_s	Number of parallel circuits	1 or 2
δ	Air gap length (minimum)	6.8mm
l_m	Length of magnet	6mm
w_m	Width of magnet	30mm
B_r	Remanence of magnet	1.29T
h_{ry}	Rotor yoke height	46mm
h_{rs}	Rotor slot height	50mm
$h_{r,enc}$	Rotor slot enclosure height	2mm
$h_{r,wedge}$	Rotor slot wedge height	2mm
b_{rt}	Rotor teeth width	8.5mm
b_{rsi}	Outer rotor slot width	5mm
b_{rso}	Inner rotor slot width	8mm
b_{ro}	Rotor slot opening	3mm

TABLE III
SIMULATION PARAMETERS FOR THE 3-PHASE CONNECTION

Symbol	Description	Value
R_s	Inner resistance of the phases	0.1Ω
ψ_m	Magnet flux linkage	359.3 mWb
e_0	3. Harmonic of zero sequence voltage	9.8V
L_d	D-axis inductance	749.9 μH
L_q	Q-axis inductance	759.5 μH
L_0	Zero sequence inductance	739.5 μH
L_s	Average self-inductance	749.6 μH
M_s	Average mutual-inductance	5.0 μH
ΔL_m	Inductance fluctuation amplitude	3.2 μH

inductances and inner resistances, and half of the magnet flux linkage. One could model the 6-phase machine in the split phase double dq system, yielding

$$\begin{bmatrix} u_{d1} \\ u_{q1} \\ u_{d2} \\ u_{q2} \end{bmatrix} = \omega \begin{bmatrix} 0 \\ \psi_m \\ 0 \\ \psi_m \end{bmatrix} + \omega \begin{bmatrix} 0 & L_q & 0 & L_{mq} \\ -L_d & 0 & -L_{md} & 0 \\ 0 & L_{mq} & 0 & L_q \\ -L_{md} & 0 & -L_d & 0 \end{bmatrix} \begin{bmatrix} i_{d1} \\ i_{q1} \\ i_{d2} \\ i_{q2} \end{bmatrix} - \begin{bmatrix} L_d & 0 & L_{md} & 0 \\ 0 & L_q & 0 & L_{mq} \\ L_{md} & 0 & L_d & 0 \\ 0 & L_{mq} & 0 & L_q \end{bmatrix} \begin{bmatrix} \frac{di_{d1}}{dt} \\ \frac{di_{q1}}{dt} \\ \frac{di_{d2}}{dt} \\ \frac{di_{q2}}{dt} \end{bmatrix} + e_{q,6} \begin{bmatrix} 0 \\ -\sin(6\omega t) \\ 0 \\ \sin(6\omega t) \end{bmatrix}, \quad (24)$$

where the torque is calculated as

$$T_e = \frac{3p}{4\omega} e_{q,6}(i_{q2} - i_{q1}) \sin(6\omega t) + \frac{3p}{4} \left[\psi_m (i_{q1} + i_{q2})\right], \quad (25)$$

where $e_{q,6}$ accounts for the q-voltage fluctuations. With zero sequence currents, it is better to use

$$T_e = \frac{p}{\omega} \left[e_{a1} i_{a1} + e_{b1} i_{b1} + e_{c1} i_{c1} + e_{a2} i_{a2} + e_{b2} i_{b2} + e_{c2} i_{c2}\right]. \quad (26)$$

Zero sequence currents will be allowed in the 6-phase rectification scheme, where

$$\begin{bmatrix} u_{01} \\ u_{02} \end{bmatrix} = \begin{bmatrix} e_{01} \\ e_{02} \end{bmatrix} - R_s \begin{bmatrix} i_{01} \\ i_{02} \end{bmatrix} - \begin{bmatrix} L_0 & 0 \\ 0 & L_0 \end{bmatrix} \begin{bmatrix} \frac{di_{01}}{dt} \\ \frac{di_{02}}{dt} \end{bmatrix} \quad (27)$$

model the dynamics. The parameters for the double dq model are found in Table IV.

TABLE IV
SIMULATION PARAMETERS FOR THE 6-PHASE CONNECTION

Symbol	Description	Value
R_s	Inner resistance of the phases	0.2Ω
ψ_m	Magnet flux linkage	372.0 mWb
Δe_{q1},Δe_{q2}	6. Harmonic of d-axis voltage	5.7V
e_{01},e_{02}	3. Harmonic of zero sequence voltage	13.9V
L_d	D-axis inductance	1120.8 μH
L_q	Q-axis inductance	1178.5 μH
L_0	Zero sequence inductance	734.6 μH
L_{ld}	D-axis leakage inductance	664.0 μH
L_{lq}	Q-axis leakage inductance	682.9 μH
L_{md}	D-axis magnetizing inductance	456.8 μH
L_{mq}	Q-axis magnetizing inductance	495.6 μH
L_s	Average self-inductance	1002.3 μH
L_l	Average leakage inductance	734.6 μH
L_m	Average magnetization inductance	276.7 μH
ΔL_m	Inductance fluctuation amplitude	19.2 μH

III. RESULTS

The DC output shows some of the fundamental performance of the rectification topologies. In order to build up the excitation current in the field winding of the generator, the rectification topologies produces an output DC voltage. Fig. 5 shows that for every electrical period, the DC voltage waveform repeats itself 6 times for the 3-phase and the 6-phase system (6-pulse topologies) and 12 times for the double 3-phase system, thereof a 12-pulse topology. The 12-pulse topology produces less harmonic content in the output DC waveform (see Table V).

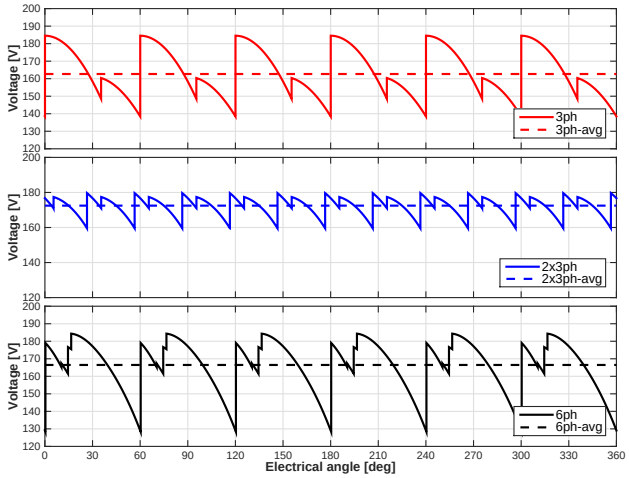

Fig. 5. Steady state loaded excitation voltage with 7 degree firing angle, plotted as a function of electrical angle, from the numerical model and with constant mechanical speed of 500 rpm

TABLE V
STEADY STATE LOADED DC VOLTAGE CHARACTERISTICS FOR THE DIFFERENT TOPOLOGIES AT FIRING ANGLE OF 7 DEGREES, FROM THE NUMERICAL MODEL

Symbol	Description	3ph	2x3ph	6ph
U_{dc}	Average dc voltage	162.7V	172.5V	166.5V
THD	Harmonic content	8.34%	2.99%	8.90%

Regarding the phase currents, Fig. 6 shows that discontinuous commutation mode is obtained in the 3-phase and the double 3-phase system, but continuous commutation happens in three of the phases in the 6-phase system. The commutation in the 6-phase system is also simultaneous on the positive and negative voltage, and up to four phases happens to conduct current at the same time. The continuous commutation causes a larger phase shift between the induced armature voltages and the phase currents, but the harmonic content in the current waveforms are greatly reduced. The numerical result in Fig. 6 causes the analytical model assumptions for the 6-phase system to not match. However, the 3-phase system and the double 3-phase system produces phase currents that matches better with the analytical square wave assumptions.

The 6-phase topology does not match well with the analytical model because of the large commutation. A large commutation is beneficial for reducing the harmonic contents in the currents, but it weakens the controllability of the excitation current. Only when the commutation process is finished in each conduction interval, the intended voltage is applied over the DC stiff load. During the commutation, the output DC voltage is a combination of the phase voltages of the commutating phases and the phase voltages of the phases conducting before the commutation was initiated. In this way, a large commutation weakens the controllability of the rectification topology. In Fig. 7, the steady state excitation current as a function of firing angle shows that the 6-phase topology is less controllable for smaller firing angles and more controllable for larger firing angles. One have to use higher firing angles to be able to change the excitation current.

Another effect of a large commutating inductance is the

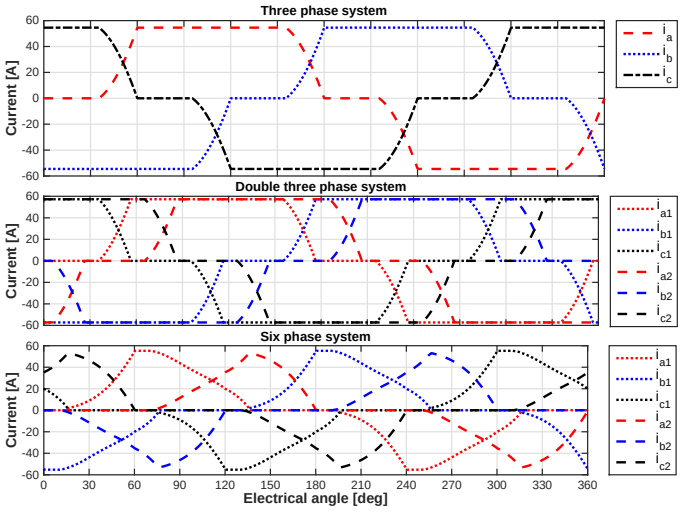

Fig. 6. Steady state phase currents for the different topologies with 7 degree firing angle, from the numerical model.

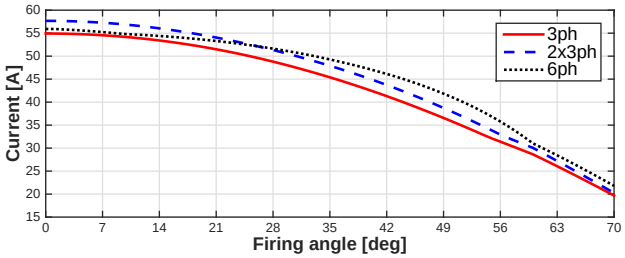

Fig. 7. Steady state excitation current as a function of firing angle for the different topologies, showing the controllability.

reduction of the maximum excitation current produced by the rectification topology, comparing the 6-phase system and the double 3-phase system. The reduction in the maximum excitation current in the 3-phase system is mainly caused by a reduced winding factor, going from 1 to 2 slots per pole per phase.

The fast step response of the excitation system is confirmed in Table VI. The natural time constant for the dc step response is 166.67ms, regarding the field winding parameters ($\tau = \frac{L_{load}}{R_{load}}$). However, the exciter rectifier is not an ideal DC stiff voltage source. The step response is faster in the numerical simulation because the average DC voltage is larger initially when excitation current is low. The 6-phase system has a 11.43ms faster time constant compared to the double 3-phase system because it reaches a lower steady state current, since the commutation begins to play a major role in the 6-phase system as the excitation current ramps up.

TABLE VI
CURRENT STEP RESPONSE RESULTS FOR THE DIFFERENT TOPOLOGIES WITH 7 DEGREE FIRING ANGLE

Symbol	Description	3ph	2x3ph	6ph
I_{dc}	Final dc current	54.55A	57.27A	55.24A
τ	Time constant	147.60ms	150.02ms	138.59ms

The fundamental frequency of the voltage ripple for each topology is actually equal to the exciter torque ripple for the same topology. The fundamental torque ripple frequency for the 3-phase and 6-phase topology is $6f_0$, but the double 3-phase system has a fundamental torque ripple frequency of $12f_0$, where f_0 is the fundamental alternating current electrical frequency. The torque ripple pulsations are plotted for all topologies in Fig. 8. Table V and Table VII shows that the harmonic content in the torque and the DC voltage tends to be lowest for the double 3-phase system.

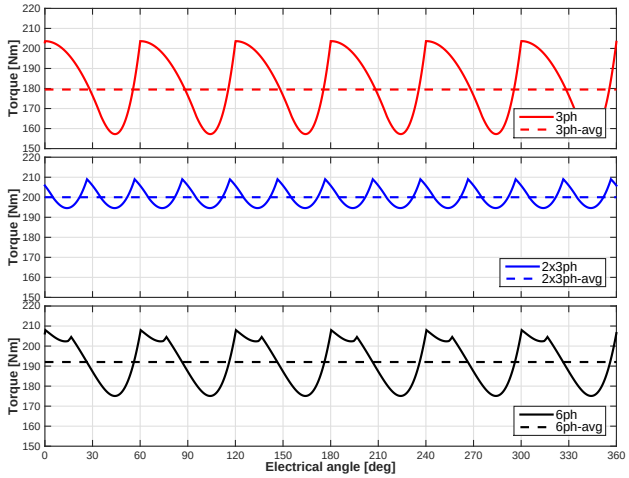

Fig. 8. Steady state torque as a function of electrical angle with 7 degree firing angle, with constant mechanical speed of 500rpm, from the numerical model.

TABLE VII
EXCITER STEADY STATE TORQUE CHARACTERISTICS WITH 7 DEGREES FIRING ANGLE, FROM THE NUMERICAL MODEL.

Symbol	Description	3ph	2x3ph	6ph
T_e	Average torque	179.49Nm	200.01Nm	192.04Nm
THD	Harmonic content	9.02%	2.28%	5.86%

Fig. 9 shows the torque ripple quantified as the total harmonic distortion, which illustrates the ratio of the amplitudes of the harmonic torque to the average torque. Not surprisingly, the double 3-phase rectifier with multilevel outputs is shown to produce the lowest torque ripple from the analytical model, when both rectification bridges are controlled with equal firing angles. With a trapezoidal voltage waveform, the torque ripple is 0 at 0 degree firing angle. However, for larger firing angles, the trapezoidal voltage produces little THD reduction compared to sinusoidal voltage waveforms. At the highest firing angles, the sinusoidal voltage produces actually a lower torque ripple for all topologies. The analytical solutions producing the plots in Fig. 9 are given in Table VIII, derived from the analytical framework developed in section II, subsection A.

The double 3-phase system gives more degrees of freedom regarding the firing angle of the rectification bridges. Fig. 10 shows that there is actually no benefit of controlling the upper and bottom thyristor bridge of the double 3-phase system with different firing angles. The contour lines tell us that the largest reduction of excitation current with the smallest possible torque ripple, happens when the firing angles are equal. The worst case in the contour plot happens when the upper and bottom bridge have a 30 degree difference in firing

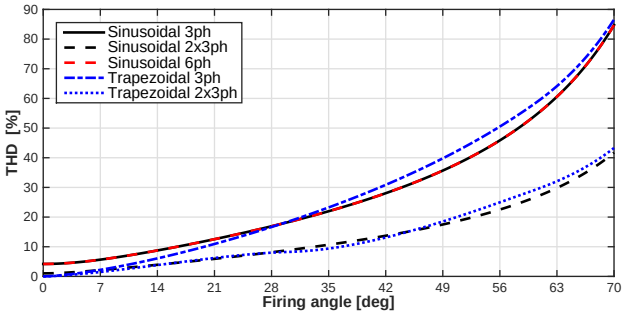

Fig. 9. Total harmonic distortion of the torque waveform in percent as a function of thyristor firing angle for different topologies, from the analytical model.

TABLE VIII
ANALYTICAL SOLUTIONS OF THE TOTAL HARMONIC TORQUE DISTORTION FOR THE DIFFERENT TOPOLOGIES

Topology	Analytical solution	Interval
3-phase/6-phase PMSM	$\sqrt{\frac{\frac{2}{3}\pi^2+\sqrt{3}\pi\cos(2\alpha)}{12\cos(\alpha)^2}-1}$	$0 \le \alpha < \frac{\pi}{2}$
Double 3-phase PMSM	$\sqrt{\frac{\frac{1}{2}\pi^2+\frac{3}{2}\pi\cos(2\alpha)}{\frac{36}{2+\sqrt{3}}\cos(\alpha)^2}-1}$	$0 \le \alpha < \frac{\pi}{2}$
3-phase BLDC	$\sqrt{\frac{1+\frac{9\alpha^2}{\pi^2}(\frac{\alpha}{\pi}-1)}{\left(1-\frac{9\alpha^2}{2\pi^2}\right)^2}-1}$	$0 \le \alpha < \frac{\pi}{3}$
	$\sqrt{\frac{\frac{7}{3}+\frac{9\alpha}{\pi}(\frac{\alpha}{\pi}-1)}{\left(\frac{3}{2}-\frac{3\alpha}{\pi}\right)^2}-1}$	$\frac{\pi}{3} \le \alpha < \frac{\pi}{2}$
Double 3-phase BLDC	$\sqrt{\frac{4+\frac{18\alpha^2}{\pi^3}(\alpha-2\pi)}{\left(2-\frac{9\alpha^2}{\pi^2}\right)^2}-1}$	$0 \le \alpha < \frac{\pi}{6}$
	$\sqrt{\frac{\frac{\alpha^2}{\pi^2}\left(\frac{54\alpha}{\pi}-45\right)+\frac{49}{12}}{\left(2-\frac{9\alpha^2}{\pi^2}\right)^2}-1}$	$\frac{\pi}{6} \le \alpha < \frac{\pi}{3}$
	$\sqrt{\frac{\frac{36\alpha}{\pi}\left(\frac{\alpha}{\pi}-1\right)+\frac{109}{12}}{\left(3-\frac{6\alpha}{\pi}\right)^2}-1}$	$\frac{\pi}{3} \le \alpha < \frac{\pi}{2}$

angle, causing the commutation of each rectification bridge to happen at the same time.

Fig. 11 compares the analytical solutions to the numerical model. The effect of the commutating inductance causes larger torque ripple for the smallest firing angles, but tends to reduce the torque ripple for higher firing angles. The plot of the torque ripple in the 6-phase system shows that the reduction of torque ripple is proportional to the size of the commutating inductance. The commutating inductance in the 6-phase system is larger because of simultaneous commutation for both the positive and negative voltage and because there is no parallel-connected phase coils.

The analytical calculation resulting in Fig. 9 comes from the assumption of a sinusoidal torque variation within each conduction interval. The 3-phase and 6-phase system has 6

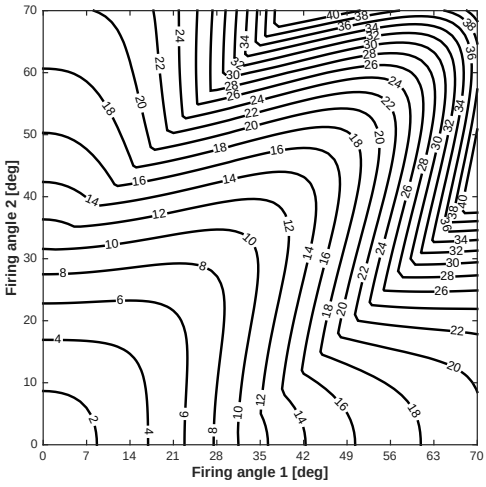

Fig. 10. Contourplot lines of the torque THD produced by the ideal double 3-phase PMSM with different fire angle combinations between the upper and bottom thyristor bridge, from the analytical model, utilizing equation (12).

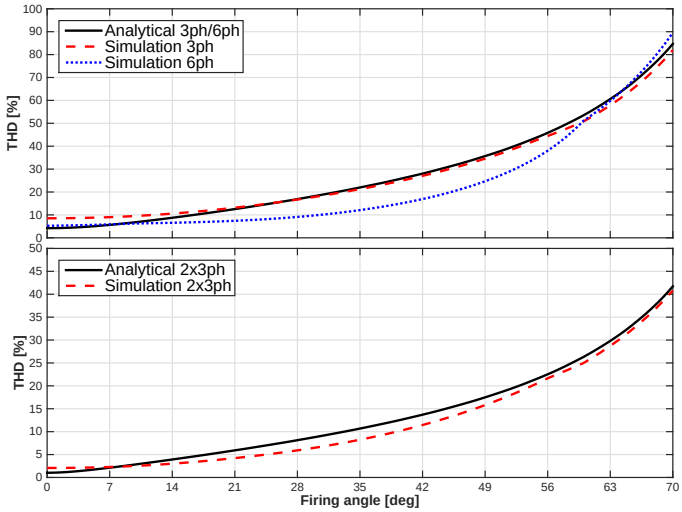

Fig. 11. Comparison in total harmonic torque distortion between the analytical model and the numerical model for the topologies of the exciter, as a function of firing angle.

different current combinations, each lasting for 60 electrical degrees. However, the double 3-phase system has 12 combinations, operating for only 30 electrical degrees each. Because of symmetry, any possible current vector within each topology, in their operating intervals, will produce the same torque function. This is shown for all topologies in Fig. 12, calculated in FEM from the Maxwell stress tensor method and compared with the analytical solutions given in Table IX. The torque functions given in Table IX, are derived from equations (23), (25) and (26). It is clear in the table that the values used, comes from the parameters in Table 3 and 4. Both methods calculate the torque with a DC stiff current load of 50A.

The zero electrical angle in Fig. 12 is defined from the point in time where a natural diode commutation will happen for that certain combination of phase currents. If the firing angle is 7 degrees, the torque function will start at 7 degrees, assuming instant commutation. In the 3-phase system, the torque function will end end at 67 electrical degrees and

jump back to 7 degrees for a new conduction interval. The double 3-phase system has a nearly identical torque function compared to the 3-phase system, however in the double 3-phase system the torque function will only last for 30 electrical degrees before it jumps to the electrical angle corresponding to the firing angle in the new interval. This is due to double amount of firing pulses per electrical period. As the firing angle increases, the torque function will produce a larger variation within the conduction interval. Since the double 3-phase conduction interval is shorter, a higher firing angle is needed in order to reach the region where the torque dips comparably to the 3-phase and the 6-phase system. The analytical results show good match with FEM. The 6-phase system has an extra term in the torque function because of the interaction with the zero sequence magnet flux linkage.

TABLE IX
ANALYTICAL TORQUE FUNCTIONS FROM THE DQ-EQUIVALENT PMSM MODEL AS A FUNCTION OF ELECTRICAL ELECTRICAL ANGLE AFTER THE NATURAL DIODE COMMUTATION, ASSUMING INSTANT COMMUTATION

Topology	Analytical solution
3-phase	$T_{3ph} = \frac{\sqrt{3}}{2} \cdot 12 \cdot 0.3593Wb \cdot 50A \cdot \cos\left(\theta - \frac{\pi}{6}\right)$
2x 3-phase	$T_{2x3ph} = \frac{\sqrt{6+3\sqrt{3}}}{4} \cdot 12 \cdot 0.372Wb \cdot 50A \cdot \cos\left(\theta - \frac{\pi}{6}\right)$
6-phase	$T_{6ph} = \frac{\sqrt{2+\sqrt{3}}}{2} \cdot 12 \cdot 0.372Wb \cdot 50A \cdot \cos\left(\theta - \frac{\pi}{6}\right)$ $-\frac{\sqrt{2}}{2} \cdot 12 \cdot \frac{13.7V}{100\pi s^{-1}} \cdot 50A \cdot \sin(3\theta)$

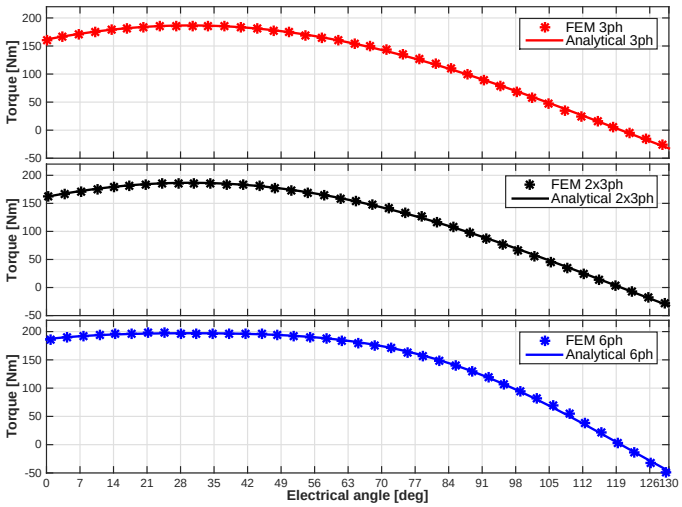

Fig. 12. Torque as a function of electrical degrees after after the natural diode commutation, assuming instant commutation.

IV. CONCLUSION

This paper investigates different active rectification topologies applied for multiphase rotating exciters. It is clear from the results that there exists certain benefits with a 6-phase rotating exciter designed for thyristor rectification topologies as the power electronic interface.

The double 3-phase exciter performs the highest reduction in torque ripple compared to the 3-phase system. However, the 6-phase system shows some reduction in the torque ripple as well and has a benefit of higher redundancy. The commutation process in the 6-phase exciter is very large, causing a reduction in the harmonic content in the phase currents, thereby reducing the torque ripple. However, the large commutation reduces the controllability of the excitation current because the output DC voltage depends more on the commutation of the phases.

A choice of permanent magnet configuration producing trapezoidal voltages, does not have a major impact on the torque ripple for normal operating firing angles above 10 degrees. The design of the exciter with respect to the equivalent commutating inductance should be a compromise between the torque ripple, the controllability and the dc voltage output.

ACKNOWLEDGMENT

The authors would like to thank Statkraft for supporting the work done, and Voith Hydro for valuable technical input.

REFERENCES

[1] F. Corbett, "Upgrading of hydrogenerator excitation systems," vol. 1, pp. 523–526, 2000.
[2] V. Ruuskanen, M. Niemelä, J. Pyrhönen, S. Kanerva, and J. Kaukonen, "Modelling the brushless excitation system for a synchronous machine," *IET electric power applications*, vol. 3, no. 3, pp. 231–239, 2009.
[3] E. Mouni, S. Tnani, and G. Champenois, "Synchronous generator output voltage real-time feedback control via strategy," *Energy Conversion, IEEE Transactions on*, vol. 24, no. 2, pp. 329–337, 2009.
[4] R. Schaefer, "Applying static excitation systems," *Industry Applications Magazine, IEEE*, vol. 4, no. 6, pp. 41–49, 1998.
[5] A. Griffo, R. Wrobel, P. H. Mellor, and J. M. Yon, "Design and characterization of a three-phase brushless exciter for aircraft starter/generator," *Industry Applications, IEEE Transactions on*, vol. 49, no. 5, pp. 2106–2115, 2013.
[6] Z. Shushu, L. Chuang, N. Yinhang, and T. Jie, "A two-stage brushless excitation method for hybrid excitation synchronous generator," *Magnetics, IEEE Transactions on*.
[7] X. Luo, T. A. Lipo *et al.*, "A synchronous/permanent magnet hybrid ac machine," *Energy Conversion, IEEE Transactions on*, vol. 15, no. 2, pp. 203–210, 2000.
[8] N. R. Zargari, Y. Xiao, and B. Wu, "A multilevel thyristor rectifier with improved power factor," *Industry Applications, IEEE Transactions on*, vol. 33, no. 5, pp. 1208–1213, 1997.
[9] A. Darabi and C. Tindall, "Brushless exciter modeling for small salient pole alternators using finite elements," *Energy Conversion, IEEE Transactions on*, vol. 17, no. 3, pp. 306–312, 2002.
[10] A. Darabi, C. Tindall, and S. Ferguson, "Finite-element time-step coupled generator, load, avr, and brushless exciter modeling," *Energy Conversion, IEEE Transactions on*, vol. 19, no. 2, pp. 258–264, 2004.
[11] M. Shahnazari and A. Vahedi, "Improved dynamic average modelling of brushless excitation system in all rectification modes," *Electric Power Applications, IET*, vol. 4, no. 8, pp. 657–669, 2010.
[12] D. C. Aliprantis, S. D. Sudhoff, B. T. Kuhn *et al.*, "A brushless exciter model incorporating multiple rectifier modes and preisach's hysteresis theory," *Energy Conversion, IEEE Transactions on*, vol. 21, no. 1, pp. 136–147, 2006.
[13] M. Shahnazari and A. Vahedi, "Analysis of brushless exciter operation in all modes of rotating rectifier," in *Industrial Electronics and Applications, 2009. ICIEA 2009. 4th IEEE Conference on*. IEEE, 2009, pp. 2377–2382.
[14] S. Haghbin, *Integrated motor drives and battery chargers for electric or plug-in hybrid electric vehicles*. PhD thesis, Department of Electric Power Engineering, Chalmers University of Technology, Gothenburg, Sweden, 2013.
[15] J. K. Nøland, *Electromagnetic Analysis of Rotating Permanent Magnet Exciters for Hydroelectric Generators*. MSc thesis, Division of Electric Power Engineering, Chalmers University of Technology, Gothenburg, Sweden, 2013.

[16] F. Evestedt, *Wireless control and measurement system for a hydropower generator with brushless exciter*. MSc thesis, Division of Electricity, Angstrom Laboratory, Uppsala University, Uppsala, Sweden, 2015.
[17] M. Tartibi and A. Domijan, "Optimizing ac-exciter design," *Energy Conversion, IEEE Transactions on*, vol. 11, no. 1, pp. 16–24, 1996.
[18] W. Shilling, "Exciter armature reaction and excitation requirements in a brushless rotating-rectifier aircraft alternator," *American Institute of Electrical Engineers, Part II: Applications and Industry, Transactions of the*, vol. 79, no. 5, pp. 394–402, 1960.
[19] H. Le-Huy, R. Perret, and R. Feuillet, "Minimization of torque ripple in brushless dc motor drives," *Industry Applications, IEEE Transactions on*, no. 4, pp. 748–755, 1986.
[20] J. Yanchao, L. Xiaobing, L. Zhuo, J. Jisheng, and L. Xinhua, "An improved passive input current waveshaping method for single-phase diode rectifier," in *Industrial Electronics, Control, and Instrumentation, 1996., Proceedings of the 1996 IEEE IECON 22nd International Conference on*, vol. 2. IEEE, 1996, pp. 695–699.

Jonas Kristiansen Nøland studied energy and environmental engineering at the Norwegian University of Science and Technology (NTNU), Trondheim, Norway, from 2009 to 2010 and received the B.S. degree in energy and environmental physics from the Norwegian University of Life Sciences (NMBU), Ås, Norway, in 2011 and the M.S. degree in electric power engineering from Chalmers University of Technology (CTH), Gothenburg, Sweden, in 2013. He is currently pursuing the Ph.D. degree in the science of electricity, engineering physics at Uppsala University (UU), Uppsala, Sweden. From august 2013 he has been working 20 percent as an assistant professor in marine electrotechnology and automation at Buskerud and Vestfold University College (HBV), Horten, Norway. Since the beginning of 2013, Jonas has focused on the study of active brushless rotating exciters for improved voltage regulation of hydroelectric generators.

Karina Bakkeløkken Hjelmervik received her PhD from University of Oslo (UiO), Oslo, Norway, in 2009 in fluid mechanics, with focus on numerical modelling, rogue waves, and tidal currents. From June 2009, she took up a position as an associate professor at Buskerud and Vestfold University College (HBV).

Urban Lundin received his PhD from Uppsala University, Uppsala, Sweden, in 2000 in condensed matter theory. He spent 2001-2004 as a post-doc at the University of Queensland, Brisbane, Australia. In 2004 he joined the division for electricity at Uppsala University. He is currently a professor in electricity with a specialisation towards hydropower systems at Uppsala University. His research focuses on synchronous generators and their interaction with mechanical components and the power system. He leads the Hydropower group and has been involved in the industrial implementation of research projects. Current research interests concerns excitation systems and magnetic bearings.